Title

Uranium speciation in acid waste-weathered sediments: The role of aging and phosphate amendments

Authors

Perdrial, Nicolas
Vázquez-Ortega, Angélica
Wang, Guohui
et al.

Publication Date

2018-02-01

DOI

10.1016/j.apgeochem.2017.12.001

Peer reviewed

Uranium speciation in acid waste-weathered sediments: The role of aging and phosphate amendments

Nicolas Perdrial[a] Angélica Vázquez-Ortega[bc] Guohui Wang[d] Masakazu Kanematsu[e] Karl T. Mueller[d] Wooyong Um[df] Carl I. Steefel[g] Peggy A. O'Day[h] JonChorover[b]

Abstract

Uranium speciation and lability are strongly coupled to mineral transformations in silicatesediments, particularly for sediments subjected to weathering in acidic, high-level radioactive waste, as occurred at the Department of Energy's Hanford (WA) site. In this study, uncontaminated Hanford sediments were reacted for 365 days with acidic (pH 3), uranium-bearing waste solutions, with and without phosphate in batch experiments, prior to detailed characterizations using electron microscopy, x-ray diffraction and x-ray absorption spectroscopy. In PO_4-reactant free systems, uranium speciation was controlled initially by precipitation of compreignacite $[K_2(UO_2)_6O_4(OH)_6{\cdot}8H_2O]$- and becquerelite $[Ca(UO_2)_6O_4(OH)_6{\cdot}8H_2O]$-like species. Subsequent further removal of uranium coincided with that of Si and accumulation of boltwoodite, $[(K, Na)(UO_2)_2O_4(HSiO_4)_2{\bullet}0.5(H_2O)]$-like species of uranium at 180 and 365 days. When present, PO_4 exerted a direct and strong control over U speciation. The detection of meta-ankoleite, $[K_2(UO_2)_2O_4(PO_4)_2{\cdot}6H_2O]$ at all reaction times when U was present emphasizes the importance of dissolved phosphate as a control on U speciation. Here, meta-ankoleite appears well crystallized and when it occurs as the principal product of sediment weathering, its low solubility is expected to limit dissolved U(VI) concentrations in groundwater. Although boltwoodite solubility is also low, it is formed more slowly (and only when PO_4 is absent), after initial precipitation of more soluble, less crystalline uranyl hydroxides. In the context of Hanford crib waste our results suggest that with PO_4 present, nearly all uranium would have precipitated in the upper soil.

Graphical abstract

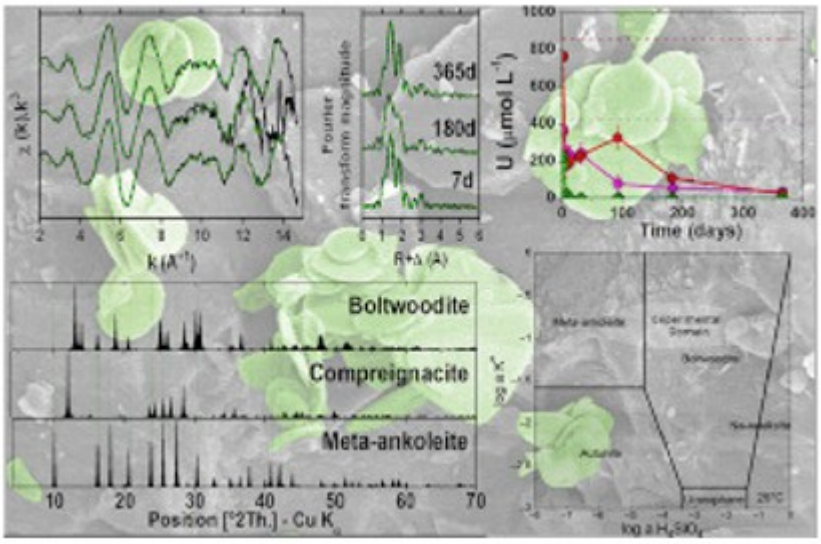

Keywords: Uranium, Hanford, Acid waste, Phosphate, Uranyl silicates

1. Introduction

The infusion of acidic uranium waste to the Hanford vadose zone represents a case study of process coupling between geochemical weathering and contaminant attenuation. Proton attack, which drives silicate mineral weathering at low pH (Oelkers et al., 2009), is controlled by proton adsorption and associated cleavage of Si-O bonds (Hellmann et al., 2012, Mantha et al., 2012). As a result, dissolution rates trend positively with H^+ concentration, and exhibit strong dependency on adsorbed proton charge density. In the context of acidic U bearing high level radioactive wastes, the co-occurrence in pore water solutions of soluble products of sediment dissolution and contaminant discharges can lead to the nucleation and crystal growth of neo-precipitates that can potentially sequester U into immobile forms.

The Hanford Site (WA, USA) covers 1518 km^2 (586 mi^2). Past nuclear weapon-production activities at Hanford resulted in approximately 1.7 trillion L (450 billion gal.) of liquid wastebeing released to the subsurface vadose and saturated zones (https://energy.gov/em/hanford-site). Initial waste-sediment reaction occurs principally in the vadose zone, and much of this liquid waste discharge occurred in the Central Plateau, a 194 km^2 (75 mi^2) area that includes approximately 800 waste sites and 900 facilities that were operated to extract and purify plutonium. The byproducts of this activity were effluentscontaminated to varying degrees with radionuclides and chemical toxicants. The most dangerous waste was stored in 177 underground tanks, and some of this waste has been released to the vadose zone. In addition, liquid waste was also discharged into engineered surface “crib” structures and allowed to percolate directly into the vadose zone. This practice resulted in large-scale contamination of the vadose zone and groundwater underlying the Central Plateau (DOE, 2012). Much of the

associated contamination remains in the vadose zone and has the potential to enter groundwater in the future, and some has already reached groundwater (Zachara et al., 2007). These crib structures now overlie inactive wastewater disposal sites in the 200 West Area and are part of the U Plant Closure Area at Hanford. The 216-U-8 crib consists of a 9 m deep excavation containing three wooden cribbed timber structures and the 216-U-12 consisting of a perforated vitrified clay pipe placed in a gravel-filled excavation about 5 m deep. Based on historical information and previous soil characterization, the vadose zone beneath both cribs is known to contain radioactive and non-radioactive contaminants (DOE, 2010). Between 1952 and 1988, uranium-containing acidic wastes resulting from acidic process condensates were discharged into the 218-U-8 and 218-U-12 cribs at the Hanford Site. This resulted in a total discharge of 380,000 m^3 of waste to 218-U-8 (operated between 1952 and 1960) and 150,000 m^3 into 218-U-12 (1960–1988). Uranium total discharge is estimated at 6500 kg for U-12 and 25,500 kg for U-8 for the entire activity period of the cribs. The pH values of the waste streams are not known precisely but readily calculated to be highly acidic (pH 2–3). Variable concentrations of PO_4 were coincident with waste discharges.

The extent of coupling between weathering and U sequestration that has occurred in the U-8 and U-12 crib locations is currently unknown. While silicate dissolution rates exhibit strong pH dependence, this dependence varies strongly with mineral type and dissolution can be non-stoichiometric due to leached surface layer formation (Casey et al., 1989, Fenter et al., 2003, Hellmann, 1997, Hellmann et al., 2012, Hochella et al., 1988, Mantha et al., 2012, Nesbitt and Muir, 1988, Schweda et al., 1997). In contrast to the surface reaction control of silicate dissolution rate, rates of dissolution for highly soluble minerals (e.g., calcite) result from a balance between surface reaction and transport control, and their respective importance varies with pH (Brantley, 2008, Plummer and Busenberg, 1987). Hence, a priori prediction of pore water compositions and neophase mineral formation – including contaminant co-precipitation – is challenging for complex mixtures such as Hanford sediments.

Whereas numerous studies have documented the pH-dependent dissolution of primary silicates and carbonates in mono-mineralic and complex Hanford sediment systems (Bickmore et al., 2001, Chorover et al., 2008, Rod et al., 2010, Mashal et al., 2004, Qafoku et al., 2004, Wan et al., 2004, Ainsworth et al., 2005, Thompson et al., 2010, Chang et al., 2011, Perdrial et al., 2011), no prior studies have assessed the weathering of multicomponent Hanford sediments under conditions representative of acidic uranium waste discharges. Since acidic discharges to the vadose zone are known to have occurred in the U-8 and U-12 locations, developing an understanding of the influence of dissolution and ensuing secondary phase precipitation reactions controlling contaminant fate is essential. We predict that mineral transformation reactions that ensue following acid waste infusion to the

subsurface will affect uranium speciation in a manner analogous to what was observed for other radionuclides in hyper-alkaline-waste-weathered systems (e.g., Chorover et al., 2008, Perdrial et al., 2011).

The behavior of U in the Hanford subsurface is influenced by its ability to form aqueous complexes, change oxidation state, and precipitate in a variety of solid phases (Maher et al., 2013, McKinley et al., 2007). Under oxic conditions, the uranyl ion ($U^{VI}O_2^{2+}$) predominates in both aqueous complexes and as an ionic species in solid phases. Spectroscopic studies of uranium-impacted field samples from Hanford cores have identified uranyl precipitated in silicate, carbonate, and phosphate phases in “microcracks” in some core samples, and as a sorbed uranyl surface complex (Brown et al., 2010, Stubbs et al., 2009, Um et al., 2010). Aging of contaminant fluids in contact with vadose zone minerals may play an important role in the dissolution of aluminosilicates and re-precipitation of uranyl-containing minerals as surface coatings or in microcracks. Prior characterization of uranium geochemistry and speciation at the Hanford site has emphasized sediments collected in the 300 Area, close to the Columbia River. This constitutes a notable difference with the conditions of the waste cribs simulated here that, located in the 200 area, were not subjected to the effects of river stage oscillations and associated redox state fluctuations.

Uranyl ions form stable aqueous complexes with carbonate and Ca, yielding carbonate, Ca-carbonate, and hydroxycarbonate species that influence uranyl sorption and uranyl mineral solubility (Grenthe et al., 1992, Guillaumont et al., 2003, Rod et al., 2012, Kanematsu et al., 2014, Gartman et al., 2015, Reinoso-Maset et al., 2017). The potential presence of phosphate as a constituent of the waste indicates that uranyl phosphate, efficient at sequestering uranium (Wellman et al., 2008), is a potential solid phase product. Homogeneous precipitation studies have shown that the presence of PO_4 controls U speciation in batch systems with the precipitation of autunite minerals whose specific types are controlled by the composition of cationic co-solutes (Kanematsu et al., 2014, Mehta et al., 2014).

Uranium speciation at Hanford has been mostly studied in the context of systems subjected to caustic, rather than acidic, waste conditions. Its sequestration into neoformed solids from caustic waste-sediment weathering is evidenced from detailed field studies. For example, uranium precipitated as boltwoodite ($Na(UO_2)(SiO_3OH)\bullet 1.5H_2O$) in the micro-fractures of U contaminated sediments under tank BX-102 (impacted by a 2.5–5.0 M Na_2CO_3, pH 10 solution) (Catalano et al., 2004, Catalano et al., 2006, McKinley et al., 2007). In the same area at Hanford, Um et al., 2010, Um et al., 2009 reported that calcium-silicates – uranophane, $Ca(UO_2)_2(SiO_3OH)_2(H_2O)_5$ - and uranyl phosphates were the main phases immobilizing U. In the 300 area, close to the Columbia River, where processing waste of a wide range of pH (1.8–11.4) has been released, studies have identified uranium phosphate (metatorbernite,

$Cu(UO_2)_2(PO_4)_2 \cdot 8H_2O$, Arai et al., 2007, Singer et al., 2009) and a rare silicate phase (cuprosklodowskite, $Cu[(UO_2)(SiO_2OH)]_2 \cdot 6H_2O$, Singer et al., 2009) as hosts for most of the uranium. In oxic enviroments (as in much of the Hanford subsurface), previous studies have suggested that solid phase U(VI) is present as the uranyl mineral schoepite ($UO_3 \cdot 2H_2O$, Duff et al., 2002). Under caustic conditions (pH 11), Duff et al. (2002)have shown that U incorporation in the hematite structure leads to its immobilization. Murakami et al. (2005) showed field evidence for nanocrystallization of uranyl-phosphate on nano-goethite and nano-hematite.

In the presence of sufficient dissolved Si, uranyl silicates are formed from supersaturated oxic solutions, as was shown when uraninite was reacted for 2 years in oxygenated ground water (Wronkiewicz et al., 1992). According to Burns (2007), uranyl silicates are the most abundant U mineral type, and these also form when spent nuclear fuel reacts with Si-enriched oxic waters, the most common group being the uranophane group.

The objective of this work was to determine the coupling between mineral transformation and U speciation and lability in acid-waste-weathered sediments subjected to a range of influent phosphate and uranium concentrations. Long-term, time series batch reactor experiments were employed to mimic the aging of fluids and solids *in situ* and to assess relations between mineral transformation and contaminant partitioning reactions postulated to have affected Hanford vadose zone sediments when the U receiving cribs were active.

2. Materials and methods

2.1. Batch reaction procedure

To simulate the aging of pristine Hanford sediment during long-term contact with acidic-radioactive-waste, we reacted 20 g of pristine (uncontaminated) sediments with 1000 g of various acid synthetic crib waste leachates (ASCW) in polypropylene bottles. The sediment was collected from the 218-E-12B Burial Ground excavation site, an uncontaminated area within the Hanford Formation (Riley and Zachara, 1992), and its detailed characterization (particle size distribution, specific surface area, cation exchange capacity, elemental composition, quantitative mineralogy) is provided in Perdrial et al. (2011). The range of compositions for ASCW solutions was based on estimated compositions of the waste streams discharged to the U-8 and U-12 cribs (CH2MHILL, 2005). Due to the variety of waste streams generated over the activity period and the lack of precise records of their actual compositions, six different ASCW solutions were used in the experiments allowing for variations of U and PO_4 concentrations and corresponding blanks. Three solutions were deprived of PO_4^{3-} and contained 0.0, 0.43 and 0.86 mmol kg^{-1} ^{238}U, respectively. The three other solutions all contained 3.0 mmol kg^{-1} PO_4^{3-} and contained 0.0, 0.43 and 0.86 mmol kg^{-1} ^{238}U, respectively. Aside from these variations, all other analyte concentrations were fixed as follows (in mmol kg^{-1} of solution, i.e., molality, *m*): 100 *m* K^+,

0.75 *m* Na^+, 2.00 *m* Cl^-, 99.5 (±2.0) *m* NO_3^- and 1.00 *m* H^+ (pH = 3). Solutions were prepared in the reactors on a mass basis using 1.8 × 10^5 Ω-m water (Barnstead nanopure), as well as reagent grade HNO_3 (0.25 M) and HCl (0.1 M) solutions and KNO_3, $NaNO_3$, and K_3PO_4 salts. After equilibration with atmospheric CO_2 via overnight bubbling, uranium was added to the solutions as $UO_2Cl_2{\cdot}3H_2O$ powder (International Bio-analytical Industries, Inc., Boca Raton, FL). Solution pH was controlled through dropwise addition of 0.25 M HNO_3. Twenty grams of uncontaminated air-dried and sieved (<2 mm) Hanford sediments were then added to the reactors. Resulting batch reactors were mixed by end-over-end rotation at 6 rpm for their respective reaction times. For each solution, 8 reactors were prepared; for two of these, 10 mL of solution was sampled and filtered at 7, 14, 30, 90, 180 d and the solid phase and solution sampled at 365 d. The remaining six reactors were stopped and entirely sampled for solution and solid phase at 7, 14, 30, 90, 180 d, respectively. This led to the analysis of batch solutions in triplicate at each sampling time and the recovery of ca. 20 g of sediment for each treatment and sampling time until 180 d of reaction. After 365 d, all reactors were sampled for both solids and solutions, and solid phase products were combined for each treatment leading to a total amount of solid of ca. 60 g of sediment reacted for 365 days. At each sampling time of each reaction system, one reactor was centrifuged at 34,155 relative centrifugal force (RCF) for 30 min (Sorvall Evolution RC), the supernatant solution was filtered through acid-washed 0.45 µm filters (GH Polypro, Pall Life Sciences), sediments were washed twice in 90% ethanol and once in a 30/70 (w/w) ethanol/water mix, and then centrifuged, prior to freezing and subsequent freeze-drying(Labconco freeze-dry system, −49 °C, 80 to 250 10^{-3} mbar). Solutions were kept at 4 °C prior to analysis and dried sediments were stored in glass vials in the dark at room temperature.

2.2. Solution analysis

Each of the sampled solutions was analyzed for pH, dissolved inorganic carbon (DIC), anions (NO_3^-, PO_4^{3-}, Cl^- and SO_4^{2-}) and metal(loid)s (Na, Mg, Al, Si, P, K, Ca, Ti, Fe, Sr, Ba and U).

Measurement of pH was performed using gel-filled electrodes to avoid contamination from the KCl filling solution (VWR symphony). Electrode calibration was performed using a four standard (pH 2, 4, 7 and 10) calibration curve.

Solution DIC was analyzed within 3 d of sampling using a Shimadzu TOC-VCSH (Houston, TX). For concentrations of selected anions (NO_3^-, PO_4^{3-}, Cl^- and SO_4^{2-}), samples were diluted in nanopure water and analyzed using an ion chromatograph (Dionex DX600, Sunnyvale, CA) equipped with an IonPac AS-22 column. For metal(loid) concentrations, samples were diluted on an analytical balance using 1% Omnitrace HNO_3 and analyzed using a Perkin Elmer Elan DRC II inductively coupled plasma mass spectrometer (ICP-MS, Perkin Elmer Elan DRC - Waltham, MA).

2.3. Solid-phase analysis

After freeze-drying, a split of each sample was ground in polyethylene containers containing 2 tungsten carbide elements using a ball mill. A split of the solid-phase sampled after 7, 180 and 365 days of reaction was subjected to fine fraction isolation. The fine fraction was concentrated by suspending 300 mg of sediments in 90% ethanol followed by sonication for 8 min. Particles remaining in suspension 2 min after the end of the sonication period were aspirated by pipette and air-dried. We selected this method over classical separation of the clay plus silt fraction by centrifugation to avoid reaction time in an aqueous liquid phase. As shown by Perdrial et al., 2011, Perdrial et al., 2014, more than 90% of the isolated particles have a diameter less than 50 μm in equivalent spherical diameter with that method.

2.4. X-ray fluorescence

For each reaction time, 0.6 g of sediment were ground and pressed into pellets (25 tons for 120 s) bound with a layer of cellulose wax (3642 Cellulose binder – SPEX SamplePrep PrepAidTM) and analyzed using a Polarized Energy-Dispersive X-ray Fluorescence spectrometer (EDXRF – SPECTRO XEPOS, Kleve – Germany) equipped with a silicon drift detector. Measurements were made under He atmosphere and four secondary targets (HOPG, Mo, Al_2O_3 and Co) were used to provide different excitation conditions as a function of voltage and current settings. Acquisition time was set to 300 s for each secondary target. Calibration of the EDXRF was performed using 12 certified reference materials and 18 Hanford sediments previously analyzed by ICP-MS following Li-metaborate fusion (Chorover et al., 2008, Perdrial et al., 2011, Thompson et al., 2010).

2.5. Scanning electron microscopy

SEM observation was performed on a Hitachi S-4800 field-emission SEM coupled with a ThermoNORAN NSS energy-dispersive X-Ray spectrometer (EDS) analysis system. A few milligrams of bulk unground sediment were sprinkled onto a conductive double-face tape and metalized with nanoparticles of platinum. Images where acquired at 15–30 kV and all analysis were acquired at 30 kV for 60s.

2.6. X-ray diffraction (XRD)

Approximately 0.05 g of ground bulk sediment and fine fraction concentrates (for 7, 180 and 365 d of reaction) were packed between two layers of Scotch Magic matte finish tape to obtain a homogeneous thin layer sample. XRD data were collected at the Stanford Synchrotron Radiation Lightsource (SSRL) on Beam Line 11–3 operating at ~12,735 eV in transmission mode, using a 345 mm radius Mar detector with a pixel resolution of 100 μm. After calibration of the detector using finely ground LaB_6 crystals, three scans were collected for each sample and added. Data were reduced using the Area Diffraction Machine software (Lande et al., 2007–2010) with a mask

covering the beamstop. The patterns were added, reduced, corrected for residual quartz saturation and systematic displacement, and converted to Cu K_α radiation wavelength. After background manual subtraction and qualitative analysis, phase mixtures extracted from the literature as well as the AMCSD and COD databases (Downs and Hall-Wallace, 2003, Gražulis et al., 2009, Gražulis et al., 2012) were modeled for scale factor, preferred orientation and peak shape (including March-Dollase factor). According to the Highscore Plus Manual, detection limit is 5 g kg^{-1}.

2.7. Time-resolved laser induced fluorescence spectroscopy

TRLIF spectroscopy was performed in a Cryo Industries RC-152 cryostat at near liquid helium temperature (LHeT) of 6 ± 1 K on the sediment and precipitate samples. At room temperature, the fluorescence spectrum for many species suffers from quenching due to impurities and other factors, but at cryogenic temperatures, the reduction of such quenching results in a sharp, intense spectrum. The samples were analyzed in a sealed 2 mm X x 4 mm fused silica cuvette. The sample cell was exposed directly to the vapor flow of liquid He, and the sample temperature was controlled by tuning both the liquid He flow rate and the electric current applied to the internal heater of the cryostat. Fluorescence emission spectra were obtained by excitation at 415 nm with the frequency doubled output of a MOPO-730 pulsed laser pumped with a Nd:YAG laser. The spectrograph wavelength was calibrated with a xenon lamp (Spectra Physics model 6033). Time-resolved fluorescence emission spectra were collected with a thermoelectrically cooled Princeton Instrument PIMAX time-gated intensified charge-coupled camera at the exit port of an Acton SpectroPro 300i double monochromator spectrograph. The data record was controlled by WinSpec data acquisition software and analyzed using IGOR software (WaveMetrics).

2.8. X-ray absorption spectroscopy

Uranium L_{III}-edge X-ray absorption spectra of the ground bulk sediments were acquired at SSRL on beam lines 11–2 and 4–1 under dedicated conditions (3 GeV, 80–100 mA). Spectra were collected using a Si(220) crystal monochromator (vertical beam size = 1 mm). On beamline 11–2, a rhodium mirror was used for harmonic rejection (17 keV cutoff energy), allowing for a fully tuned beam. On beamline 4–1 the beam was detuned to 60% of maximum intensity to reduce harmonic content. Beam energy was calibrated with a Y^0standard by assigning the first inflection on the K-edge to 17,038 eV and with a secondary UO_2(s) standard with the energy at the midpoint of the edge jump set to 17,166 eV. Sediments were packed evenly in aluminum holders, sealed with Kapton tape and held in a N_2 cryostat at 5–15 K during data collection. Fluorescence absorption spectra were collected using a solid-state 100 element Ge-array detector on BL 11–2 or a 30 element Ge detector on BL 4–1, and successive scans (6–12) were averaged.

Data were analyzed using the programs Sixpack (Webb, 2010), Athena (Ravel and Newville, 2005) and EXAFSPAK (George and Pickering, 2000). Absorption background was subtracted using a linear fit through the pre-edge region and normalized to the average height of the post-edge jump. Normalization was extended into the EXAFS region (above threshold energy $k = 0$ Å^{-1} set to 17,175 eV) using a cubic spline. Sediment fine fraction (FF) spectra were analyzed by least-squares linear combination (LC) fits using reference compound spectra to determine the primary U-bearing phases. The reference spectra used in final LC were selected based on XRD analysis of the sediments and had been previously analyzed and modeled in Kanematsu et al. (2014). The data range for LC fits was consistently from $k = 2$ to 12 Å^{-1}.

2.9. Sequential extraction procedure

Portions of the sediments reacted for 180 and 365 d were subjected to a four-step sequential extraction (SE) scheme, summarized in Supporting Information Table 1 (adapted from McKeague and Day, 1966, Begin and Fortin, 2003, Dold, 2003, Zhou and Gu, 2005, Chorover et al., 2008). Sequential chemical extractions were performed in five replicates on 1.0 g mass of freeze-dried sediment. The SE scheme resulted in five distinct U pools representing variable labilities by targeting those phases soluble in: pure water (Step 1), Na bicarbonate solution (Step 2), ammonium oxalate solution (Step 3), acid soluble pool (Step 4), the residual solid phase pool, consisting mainly of silicate minerals (SI Table S1). Each extraction step (except Step 1) was followed by a rinse with ultrapure water (18.2 MΩ cm) for 20 min with a 1:20 solid to solution mass ratio at room temperature. Extractions and rinses were shaken at 100 rpm followed by centrifugation at 18,500 RCF for 20 min and finally filtered through a 0.2 µm acid washed cellulose acetate membrane. The rinses were combined into the supernatant solutions for each extraction, with the remaining solids subjected to further extraction. Soil-free controls (‘blanks’) were carried out in triplicate. After each of steps 2 and 3, a replicate was sacrificed and subjected to solid-phase characterization. The average and standard deviation values for steps 1, 2, 3, and 4 were therefore calculated based on 5, 5, 4, and 3 replicates, respectively. U and major elements (Al, Fe, Mn, Mg, Ca, K, P, and Si) in the extracted solutions were determined by ICP-MS.

2.10. Thermodynamic modeling

Aqueous speciation and saturation indices of solutions with respect to various solid phases were calculated for the experimental conditions the software program Geochemist's Workbench 7.0® (GWB). Thermodynamic data included a modified version of the Lawrence Livermore National Laboratory (LLNL) database thermo.com.v8.r6+ amended with the latest critically-reviewed stability constants of aqueous U(VI) species (Kanematsu et al., 2014) and solubility

products (K_{sp}) of U(VI) solids. Activity coefficients were calculated using the Davies equation.

3. Results

3.1. Solution chemistry

Interaction with sediment resulted in rapid neutralization of acidic waste solutions (Fig. 1a). While all ASCW solutions were initially set to pH 3, upon reaction, solution pH increased to near-neutral values after only 7 d of reaction. After 90 d of reaction, solution pH stabilized at a value of 7.0 (+-0.2) when PO_4 was included in the ASCW and at 7.6 (+-0.3) when it was absent (Fig. 1a). Solutions also became rapidly enriched in DIC upon reaction with the sediments, stabilizing after 90 d (Fig. 1b). In the absence of added PO_4 and presence of U in the reactant solution, DIC concentrations were double those of systems free of PO_4 or U. Dissolved U concentration decreased to the nano-molar range after only 14 d of reaction in PO_4–reactant systems (Fig. 1c). In PO_4-reactant free systems, however, a larger fraction of the initial dissolved U remained in solution at each sampling point, decreasing slowly to a value of 30 ± 15 mmol l^{-1} independent of the initial U concentration (Fig. 1). Whether U was present or not, concentration of added PO_4 decreased steadily with reaction time in the PO_4systems while small amounts of PO_4 were detected at 90 d in the PO_4-reactant free systems (Fig. 1d).

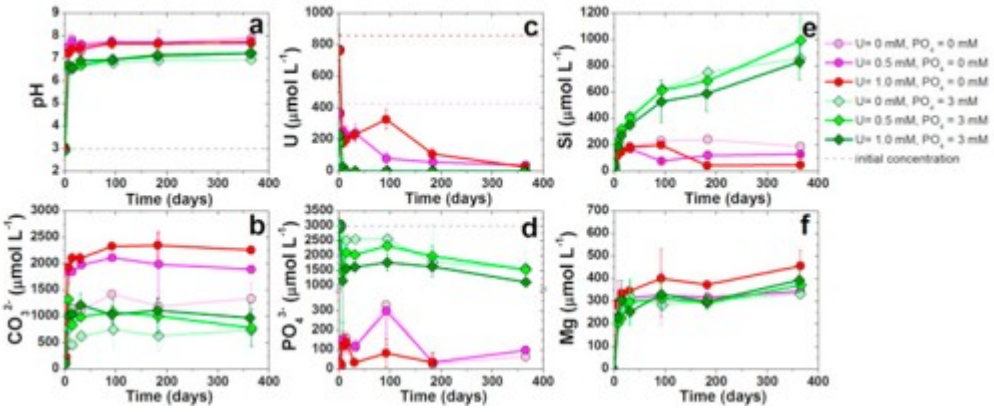

Fig. 1. Evolution of solution chemistry during reaction for pH (a), Total inorganic carbon reported as CO_3^{2-}(b), U (c), total PO_4^{3-} (note the break on the y-axis) (d), Si (e) and Mg (f). Note the y-axis break for panel d.

Concentrations of dissolve silicon also showed strong dependence on the presence or absence of PO_4 addition (Fig. 1e). Irrespective of U concentration, when PO_4 was present, aqueous Si concentration increased steadily over the course of the experiment to reach 800–1000 µmol kg^{-1} after 365 d of reaction. Without added PO_4, Si release to solution was significantly lower after 30 d and throughout the remainder of the experiment. Further, without added PO_4, U concentration also influenced Si behavior. With zero U addition, aqueous Si concentration increased initially and then stabilized at ca. 200 µmol kg^{-1}. With U present (but no

PO_4 addition), the increase in Si concentration was followed by a subsequent decrease between 30 and 90 d (for 0.43 mmol kg^{-1} U) or between 90 and 180 d (for 0.86 mmol kg^{-1} U) (Fig. 1e). Magnesium concentrations increased sharply at first and then remained steady for the remainder of the experiment, irrespective of U or PO_4 addition (Fig. 1f).

3.2. Solid phase analysis

3.2.1. X-ray fluorescence

XRF data on the sediments as a function of time and treatment corroborated those derived from solution phase analyses (Table S2, Supplemental Information). Uranium was incorporated into the sediments at amounts that correlated with starting concentrations in solution (Table S2). The U concentration measured in the sediments represented the incorporation of 40–100% of U added. XRF also detected the concurrent solubilization of Mg, Si, Ca and Fe and incorporation of Na and K in the sediments upon reaction.

3.2.2. X-ray diffraction

Initial analysis by XRD of the bulk sediments did not reveal detectable or quantifiable differences in mineralogy of the reacted sediments compared to unreacted sediments, and for this reason XRD of the fine fraction concentrates was performed to enhance sensitivity (Fig. 2 & Table S3). Assuming that the fine fraction isolates effectively concentrated all neo-formed uranium phases, we calculated the fraction of U-bearing minerals in the actual sediments by applying the dilution factor to the quantitative estimates irrespective of mineral densities (Table 1). Analysis of the PO_4-reactant free systems where U was present revealed early (7 d) uranium oxyhydroxide [compreignacite $K_2(UO_2)_6O_4(OH)_6{\cdot}7H_2O$ or becquerelite $Ca(UO_2)_6O_4(OH)_6{\cdot}8H_2O$] and boltwoodite [$(K,Na)_2(UO_2)_2(HSiO_4)_2{\bullet}0.5H_2O$] precipitation (Fig. 2a,c), with mass fractions of these neo-phases increasing with time (Table 1). No other crystalline U phase was detected in the absence of added PO_4. When PO_4 was added, the only crystalline U phase detected was meta-ankoleite [$K_2(UO_2)_2(PO_4)_2{\cdot}6H_2O$], which appeared early in the time series (Fig. 2 b,d). While no trend in the amount of precipitate was observed with time, the amount of crystalline meta-ankoleite was higher in the 0.86 mmol kg^{-1} U systems than in the 0.43 mmol kg^{-1} systems (Table 1).

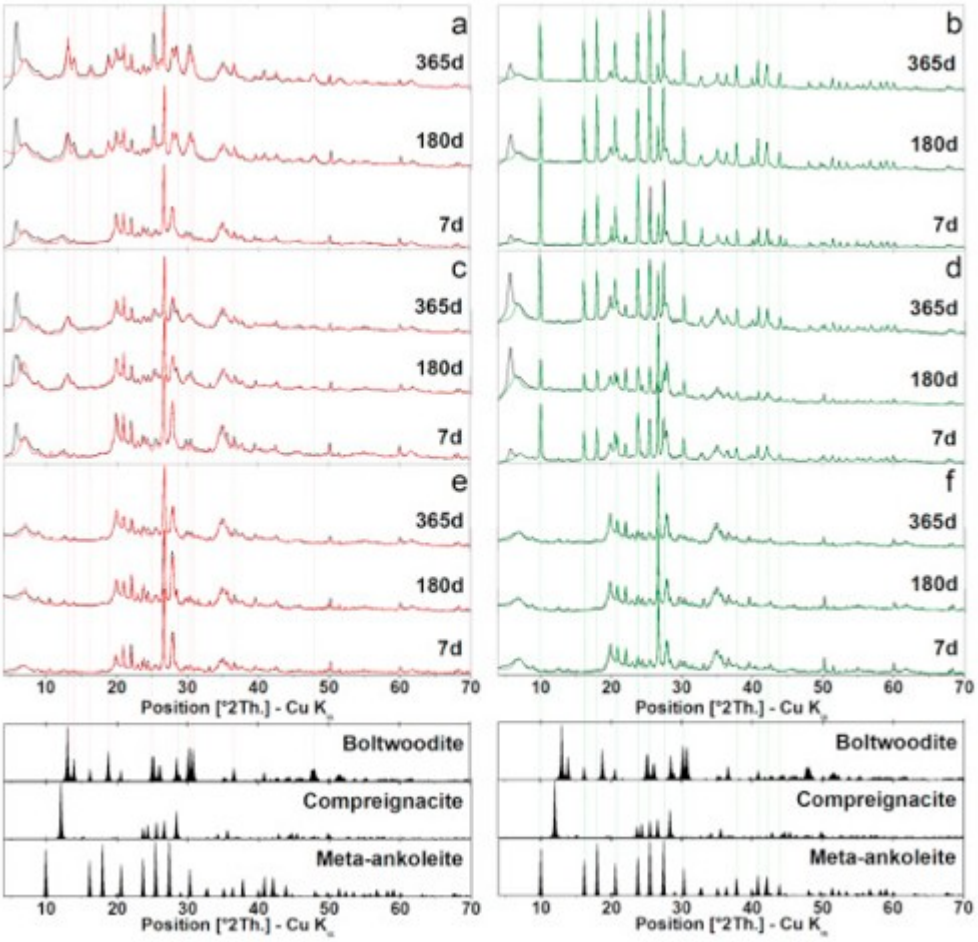

Fig. 2. Synchrotron x-ray diffractograms of the concentrated fine fraction of the sediments at 7, 180 and 365 days reacted with 1 mM U and no PO_4 (a), 1 mM U and 3 mM PO_4 (b), 0.5 mM U and no PO_4 (c), 0.5 mM U and 3 mM PO_4 (d), no U and no PO_4 (e), no U and 3 mM PO_4 (f). Lower diffractograms are simulations generated from published structures.

Table 1. Estimated percent of uranium phases in the bulk sediments inferred from the XRD quantification of the reacted fine fraction concentrates.

	Compreignacite (K,Ca,Na) $(UO_2)_6O_4(OH)_2 \cdot 8(H_2O)$	**Boltwoodite (K, Na) $(UO_2)_2O_4(HSiO_4)_2 \cdot 0.5(H_2O)$**	**Meta-ankoleite $K_2(UO_2)_2O_4(PO_4)_2 \cdot 6(H_2O)$**
U = 0.5, PO_4 = 0, 7d	0.08	–	–
U = 0.5, PO_4 = 0, 180d	–	1.06	–
U = 0.5, PO_4 = 0, 365d	–	3.74	–
U = 1.0, PO_4 = 0, 7d	0.23	–	–
U = 1.0, PO_4 = 0, 180d	–	1.10	–
U = 1.0, PO_4 = 0, 365d	–	2.12	–
U = 0.5,	–	–	2.61

	Compreignacite $(K,Ca,Na)(UO_2)_6O_4(OH)_2 \cdot 8(H_2O)$	Boltwoodite $(K, Na)(UO_2)_2O_4(HSiO_4)_2 \cdot 0.5(H_2O)$	Meta-ankoleite $K_2(UO_2)_2O_4(PO_4)_2 \cdot 6(H_2O)$
PO_4 = 3, 7d			
U = 0.5, PO_4 = 3, 180d	–	–	1.94
U = 0.5, PO_4 = 3, 365d	–	–	5.09
U = 1.0, PO_4 = 3, 7d	–	–	10.24
U = 1.0, PO_4 = 3, 180d	–	–	14.30
U = 1.0, PO_4 = 3, 365d	–	–	12.03

3.2.3. Scanning electron microscopy (SEM) imaging

Observation of the reacted sediments by SEM as a function of reaction time (7, 180, 365 d) did not reveal the presence of detectable uranium in the PO_4-reactant free systems. However, with added PO_4, native minerals were covered by thin platy particles of a size ranging between 1 and 5 μm in equivalent diameter and containing uranium, potassium and phosphorus identified as meta-ankoleite precipitates (Fig. 3).

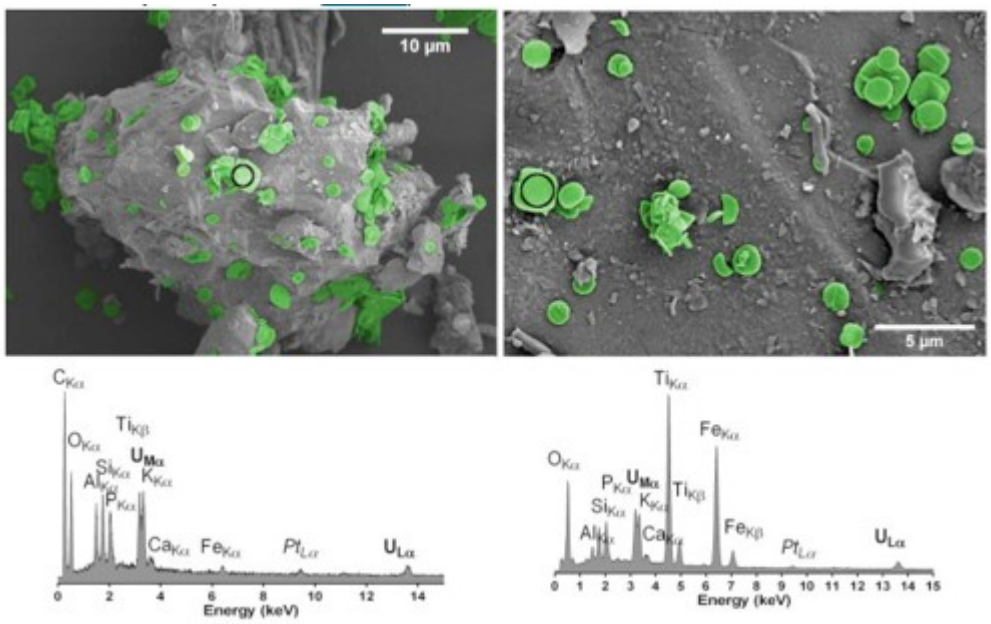

Fig. 3. SEM microphotographs of selected area of the sample reacted for 180d with 3 mM PO_4 and 0.5 mM U (left) and 3 mM PO_4 and 1 mM U (right) and EDS analyses of the precipitates circled on the images. Images have been artificially colored to represent uranium-phosphate precipitates in green. Platinum peaks (Pt) in the EDS result from the coating added to make the sample conductive. (For interpretation of the references to color in this figure legend, the reader is referred to the Web version of this article.)

3.2.4. Time-resolved laser induced fluorescence spectroscopy

Weathered bulk sediments from selected reaction times (7, 180 and 365 d) were analyzed by time-resolved infra-red light fluorescence spectroscopy and compared with spectra of uranium-bearing references. In the presence of added PO_4, spectra were consistent, independent of the initial U amount and the reaction time, corresponding to a reference U phosphate signature (Fig. 4). However, in the absence of added PO_4 and at both initial U concentrations, TRILFS spectra showed appearance and progressive growth of a 510 nm peak between 180 and 365 d, giving spectra that were similar to the boltwoodite spectrum at the end of the reaction period. The TRILFS spectra at 7 d for the PO_4-reactant free systems could not be matched to spectra of reference minerals from this study or published spectra.

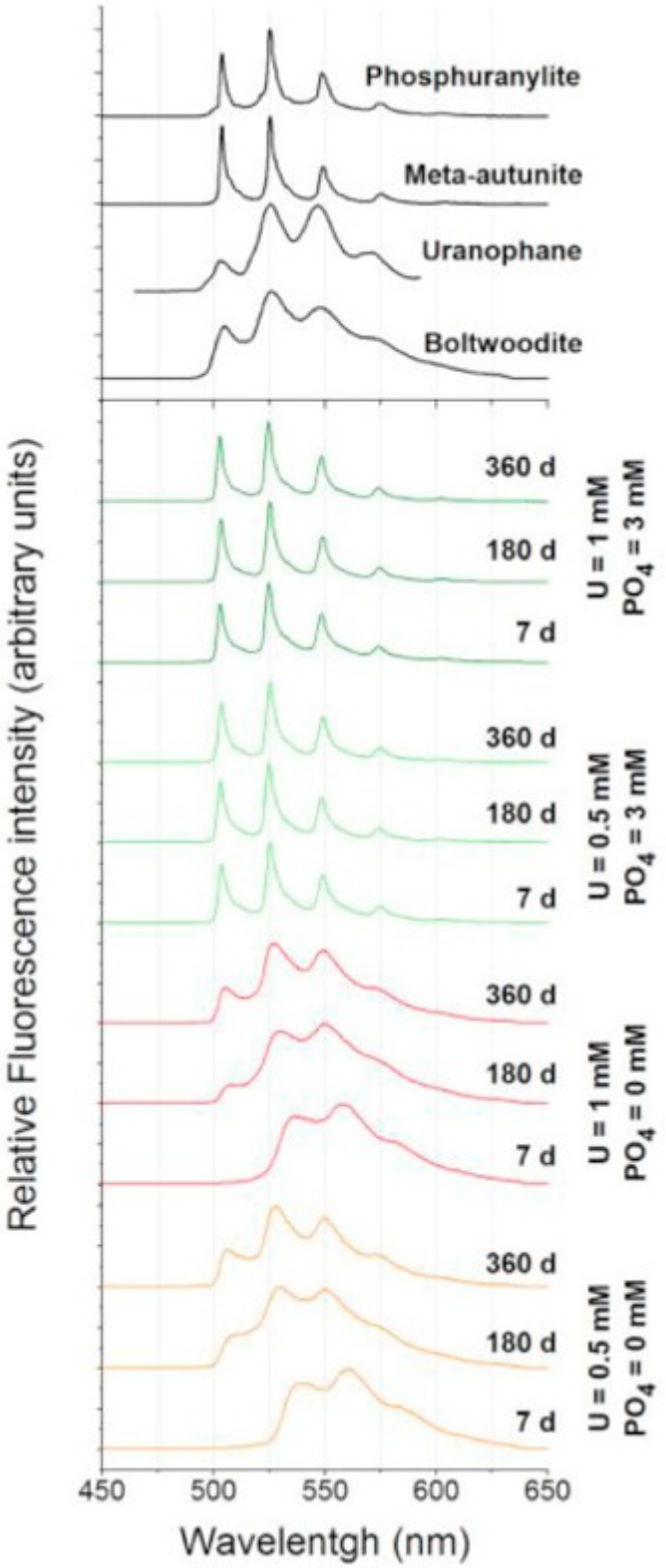

Fig. 4. TRILFS analysis of model uranium compounds (black lines) and fine fraction concentrates of sediments reacted for 7, 180 and 365 days under the different treatments.

3.2.5. Extended X-ray absorption fine structure (EXAFS) spectroscopy

The evolution of U solid phase speciation was monitored by U L_{III}-edge EXAFS analysis of the sediments at 7, 180 and 365 d (Fig. 5). In LCF fits, which were not forced to sum to unity, the sum of components deviated from 1.0 due to differences in crystallinity, matrix effects, and data quality (signal/noise) between standard and unknown spectra. This comparison provides an indication of the accuracy of the LCF approach for identifying components that contribute to EXAFS backscattering in the sample spectra (mean error ±10%). In the absence of added PO_4, spectra are dominated by U-O shells, with differences in the speciation of U being reflected in more distant shells. Of particular interest, the EXAFS signal between 9 and 13 $Å^{-1}$ allowed for linear combination fitting of the reacted sediment spectra to spectra of reference U minerals from Kanematsu et al. (2014). Uranium in these samples was principally present in a U-oxyhydroxide phase, mostly compreignacite with a smaller contribution from becquerelite- or schoepite-type coordination, and boltwoodite-type coordination (Table 2). Of particular note was the increase in boltwoodite-like coordination at the expense of compreignacite-like as a function of reaction time.

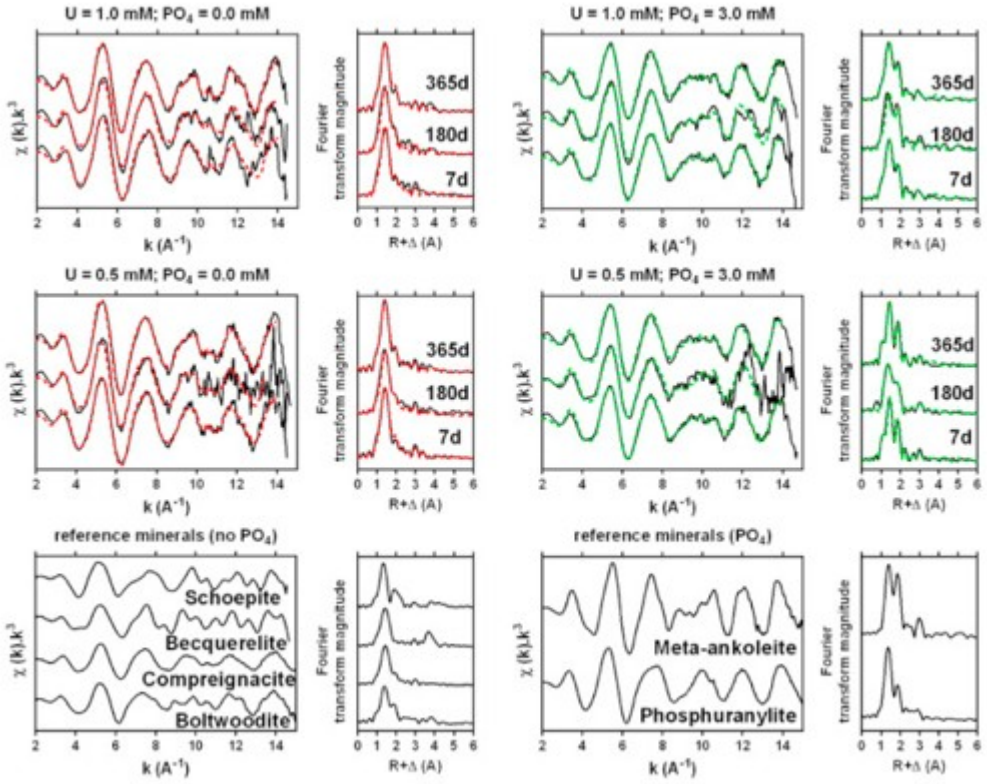

Fig. 5. U L_{III} edge EXAFS spectra and corresponding Fourier transform of model uranium compounds (bottom) from Kanematsu et al. (2014) and sediments reacted for 7, 180 and 365 days under the different treatments. Black lines represent the experimental spectra and dotted colored lines are the results of linear combination fits reported in Table 2.

Table 2. Linear combination fits (LCF) of U L_{III}-edge EXAFS spectra to give component fractions (numbers in brackets represent the fraction error).

Sample	Reaction time (d)	Compreignacite	Becquerelite	Schoepite	Boltwoodite	Phosphuranylite	Meta-ankoleite	Sum	Red. χ^{2a}
U = 0.5 mM PO_4 = 0.0 mM	7	0.74 (0.08)	0.13 (0.04)	–	0.21 (0.05)	–	–	1.08 (0.17)	0.19
	180	0.70 (0.13)	0.10 (0.07)	–	0.21 (0.00)	–	–	1.01 (0.20)	0.50
	365	0.57 (0.07)	0.14 (0.04)	–	0.44 (0.04)	–	–	1.15 (0.15)	0.14
U = 1.0 mM PO_4 = 0.0 mM	7	0.81 (0.00)	0.14 (0.04)	0.14 (0.04)	–	–	–	1.09 (0.10)	0.43
	180	0.55 (0.10)	0.21 (0.06)	–	0.16 (0.07)	–	–	1.08 (0.23)	0.35

Sample	Reaction time (d)	Compreignacite	Becquerelite	Schoepite	Boltwoodite	Phosphuranylite	Meta-ankoleite	Sum	Red. χ^{2a}
	365	0.65 (0.00)	–	–	0.47 (0.03)	–	–	1.12 (0.03)	0.12
U = 0.5 mM PO_4 = 3.0 mM	7	0.56 (0.04)	–	–	0.14 (0.04)	–	0.43 (0.00)	1.13 (0.08)	0.16
	180	–	–	0.12 (0.10)	–	0.26 (0.13)	0.62 (0.13)	1.00 (0.36)	0.94
	365	0.11 (0.08)	0.25 (0.04)	–	0.31 (0.05)	–	0.51 (0.02)	1.18 (0.19)	0.20
U = 1.0 mM PO_4 = 3.0 mM	7	0.39 (0.08)	0.13 (0.04)	–	0.20 (0.05)	–	0.47 (0.02)	1.19 (0.19)	0.17
	180	–	0.27 (0.04)	–	0.13 (0.04)	–	0.69 (0.00)	1.09 (0.0	0.50

Sample	Reaction time (d)	Compreignacite	Becquerelite	Schoepite	Boltwoodite	Phosphuranylite	Meta-ankoleite	Sum	Red. χ^{2a}
								8)	
	365	0.33 (0.08)	0.16 (0.04)	–	0.14 (0.05)	–	0.52 (0.02)	1.15 (0.19)	0.20

a Error as provided by Athena (Ravel and Newville, 2005).

In the presence of added PO_4 the EXAFS spectra were similar to each other, displaying two oxygen shells indicative of six-fold coordinated uranium with axial and equatorial U-O bonds and more distant U-P shells (Fig. 5). Uranium in these reacted sediments has dominantly a meta-ankoleite-like coordination with smaller amounts of compreignacite-, becquerelite- and boltwoodite-like coordination. In one instance (presence of PO_4 and 0.5 mM U) a lower quality spectrum was better fit with phosphuranylite and schoepite in addition to the dominant meta-ankoleite-like coordination (Fig. 5 and Table 2).

3.2.6. Sequential extraction

Solid phase samples isolated after 180 and 365 d of reaction with ACSW solutions were subjected to a sequential chemical extraction procedure to quantify the U mass fraction associated with i) water soluble, ii) bicarbonate extractable, iii) oxalate extractable, iv) acid soluble, and v) residual pools to measure U lability as a function of treatment and time (Fig. 6a). These steps target, in the same order as above, the i) water soluble phases, ii) phosphate-, carbonate- and silicate-bound U, iii) amorphous oxide phases, iv) strong-acid soluble minerals and iv) the refractory minerals. For sediments reacted in the presence of added PO_4, nearly all U was extracted during the bicarbonate extraction step (99.1% and 103.3% U for 180 and 360 d, respectively). The U present in PO_4-reactant free sediments showed a different lability that varied with reaction time with 74.6% and 94.6% U present in the bicarbonate extractable fraction for 180 and 365 d of reaction, respectively (Fig. 6). An important U fraction in the PO_4-reactant free sediments at 180 and 365 d remained in the residual of the sequential extraction protocol (30% and 12%, respectively).

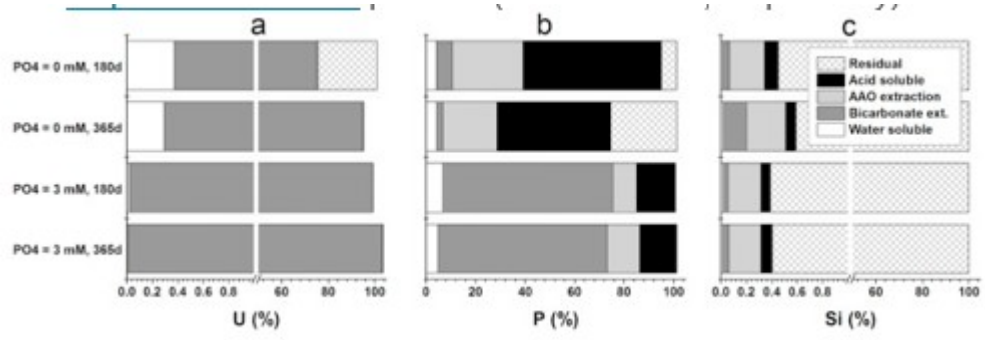

Fig. 6. Percentage of total U, P, and Si released during sequential extraction. Sequential extractions were only performed on the sediments reacted with 0.86 mM U.

In the presence of added PO_4, P was associated to a higher extent with the bicarbonate extractable pool (68.5% and 68.2% of total P at 180 and 365 d, respectively) followed by acid soluble (15.8% and 15.0% of total P at 180 and 365 d, respectively), amorphous (9.9% and 13.1% of total P at 180 and 365 d, respectively), and water soluble (6.8% and 5.0% of total P at 180 and 365 d, respectively) pools (Fig. 6b). Bicarbonate extractable P in the PO_4reactant-free system was 3.4% and 0.75% for 180 and 365 d,

respectively. According to the mass balance calculation, after the sequential extraction, no P remained in the residual pool for the PO_4 added systems. Silicon concentrations in all treatments were largely associated with the residual pool ranging from 99.55% to 99.64% (Fig. 6c). A small Si fraction was associated with the bicarbonate extractable pool (which dissolved a large amount of U), suggesting the possible dissolution of uranyl-silicates. The bicarbonate extractable Si in the system with added PO_4 at 180 and 365 d was 0.03% and 0.04% of the totals, respectively and in the PO_4 reactant-free system was 0.04% (180 d) and 0.11% (365 d) of the totals, respectively (Fig. 6c). Patterns for Mg, Al, K, Ca, Mn and Fe are included in the SI (Fig. S1). In summary, the sequential extraction shows that most of the U is extracted during the bicarbonate extraction step, along with P when it was added, and it is not correlated with other major element when P was not added. This suggest that U is present mostly bound to PO_4 in PO_4-amended systems and as hydroxide in the absence of added PO_4. The fairly high U fraction present in the residual fraction of the sample reacted without PO_4 for 6 month is not explained given the low initial U in the sediment. It could be attributed to the presence of a specific U-bearing phase not targeted in any step of the extraction.

4. Discussion

4.1. Weathering dynamics

Weathering of Hanford sediments upon contact with acidic uranium waste is initially controlled by acid-base reaction. Upon contact with the reacting solution deprived of U and PO_4, a very rapid buffering of pH (Fig. 1a), associated with quick carbonate release (Fig. 1b) and the disappearance of calcite (Table 1) indicates proton consumption by carbonate dissolution (Eq. (1)).

(1)$CaCO3(s)H+aq→Ca2+(aq)+HCO3−(aq)$

While initial Si release is rapid, the plateau at 200 μmol L^{-1} (Fig. 1e) indicates a decreasing rate of proton consumption consistent with neutralization of solution pH. Sediment weathering in the presence of PO_4 also shows a rapid buffering of pH (Fig. 1a) associated carbonate and silicate dissolution (Fig. 1b,e; Table 1). However, pH stabilizes at a slightly lower level, consistent with less carbonate release (Fig. 1 a,b), but a steady Si increase to values four times higher than in the absence of added PO_4 (Fig. 1e). Lack of difference in Mg release with or without PO_4 addition indicates that the steady Mg release is due to ion exchange reactions. Because the PO_4 is added as $H_2PO_4^-$, which has a pKa of 7.2 (second dissociation of phosphoric acid), it donates protons to buffer solution pH as protons are consumed in carbonate weathering. This explains the slightly lower pH in presence versus absence of phosphate.

4.2. Uranium solid phase speciation

4.2.1. PO_4 reactant free systems

In systems devoid of added PO_4, experimental results indicate that U aqueous speciation is initially controlled by pH neutralization from calcite dissolution that promotes hydrolytic formation of uranium oxyhydroxides. In these systems, a large fraction of added U was removed from solution at early reaction time, leaving ca. 200 μmol L^{-1} of dissolved U irrespective of starting concentration at 7–30 d (Fig. 1c). Carbonate release increased with U concentration in the ASCW solution (Fig. 1b). This suggests an initial acid-base reaction where uranyl-promoted hydrolysis and precipitation yields protons to enhance carbonate weathering (eqs. (2), (3), Gorman-Lewis et al., 2008). This is confirmed by the detection of compreignacite [$K_2(UO_2)_6O_4(OH)_6 \cdot 7H_2O$] and becquerelite [$Ca(UO_2)_6O_4(OH)_6 \cdot 8H_2O$]-type of U species by linear combination fits of the U L_{III} EXAFS (Table 2) and the presence of crystalline compreignacite detected by XRD (Table 1) at 7 d of reaction.

Beginning at 30 d of reaction in the absence of added PO_4, the behavior of U in solution is very similar to that of silicon (Fig. 1e). Ensuing removal of uranium from solution corresponds that of silicon between 30 and 90 d for the 0.43 mM ^{238}U system and between 90 and 180 d for the 0.86 mM ^{238}U system. This suggests that after initial U precipitation into hydroxylated phases, a uranium silicate phase precipitates when a threshold Si concentration is reached (Eq. (4)). This is confirmed by solid-phase molecular and micro-scale speciation analysis of the samples that (i) revealed formation and growth of a boltwoodite [$(K,Na)UO_2(HSiO_4) \cdot H_2O$] -like phase of U beginning at 180 d (U EXAFS data, Table 2), (ii) a boltwoodite signature in TRILFS (Fig. 4), and (iii) the identification and accumulation of this mineral as observed by XRD (Tables 1 and S2) after 180 d of reaction.

(2) $2K^+ + 6UO_2^{2+} + 17H_2O \rightarrow K_2(UO_2)_6O_4(OH)_6 \cdot 7H_2O + 14H^+$

(3) $Ca^{2+} + 6UO_2^{2+} + 18H_2O \rightarrow Ca(UO_2)_6O_4(OH)_6 \cdot 8H_2O + 14H^+$

(4) $0.5Na^+ + 0.5K^+ + H_4SiO_4(aq) + UO_2^{2+} + H_2O \rightarrow (Na,K)UO_2(HSiO_4) \cdot H_2O + 3H^+$

Geochemical modeling of the PO_4-reactant free systems showed that solutions became rapidly supersaturated with respect to uranium phosphate, carbonate, and silicate phases in high bicarbonate systems (Fig. 7). Later, as pH increases, supersaturation values decrease with solutions remaining slightly oversaturated with respect to uranium phosphate and carbonate.

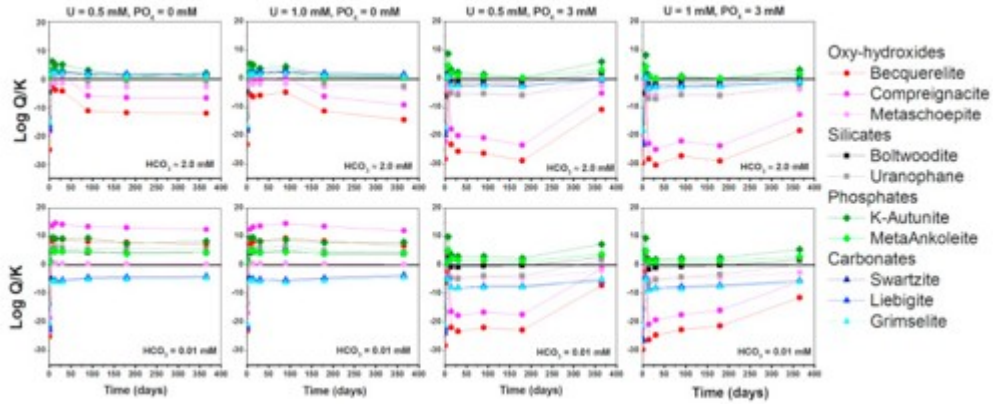

Fig. 7. Evolution of the saturation index (log Q/K) of uranium minerals in the experimental systems.

Our solid phase characterization results show that U is present as oxyhydroxide and later as silicate phases when release of silicon from initial weathering provides sufficient Si to promote boltwoodite precipitation (Table 1, Table 2, Fig. 2, Fig. 4, Fig. 5). The lack of spectroscopic evidence for solid-phase uranyl carbonates indicates a modeling over-prediction for their precipitation in our system. Although we used critically-evaluated thermodynamic data for common uranyl carbonates phases (swartzite, liebigite, grimselite, extracted form Alwan and Williams, 1980), several authors have questioned their validity, and any inaccuracies may have impacted our modeling results as well. In particular, Grenthe et al. (1992) considered the thermodynamic data reported by Alwan and Williams (1980) for the liebigite group minerals unreliable and Chen et al. (1999) suggested that the solubility product of liebigite may be erroneous. Furthermore, some in-gassing of CO_2 may have contributed to this discrepancy. Indeed, studying the effects of increasing pH (from 3 to 6) on U speciation in acidic sediments, Tang et al. (2013) showed that headspace CO_2 had a large impact on U speciation with its precipitation into liebigite suggested by geochemical modeling. Considering the amount of calcite available in the starting material (31 g kg^{-1} at most, Table S2) as the principal source of carbonate in the system, calculations reveal that the measured concentration of dissolved carbonate (2 mmol L^{-1}) exceeds the amount attributable to calcite dissolution alone (0.01 mmol L^{-1}). While some CO_2 in-gassing certainly occurred during the experiment, additional in-gassing likely occurred upon sampling. Without these atmospheric contributions, phase stability and uranium speciation indicate that the solutions would be undersaturated with respect to uranyl carbonates and oversaturated with respect to uranyl oxyhydroxides, phosphates and silicates (the latter because of diminished prevalence of uranyl-carbonate aqueous complexes), in particular for compreignacite at early reaction times (Fig. 7). In addition, in the low carbonate conditions and in the presence of sufficient dissolved silicon, boltwoodite is the most stable uranium phase in our experimental domain (Figs. S2c and S3c). The two bicarbonate concentrations depicted in the top and bottom row of Fig. 7 can be

considered to bracket those that were present during the mineral transformation reactions, and our solid phase characterization data suggest that either the thermodynamic data for uranyl carbonate solids are inaccurate or that precipitation of oxyhydroxides, phosphates and silicates is kinetically favored.

4.2.2. PO_4-amended systems

When present, PO_4 exerted a direct and strong control over U solid phase speciation. Here, nearly all U was immobilized upon introduction (Fig. 1c). Concomitantly, PO_4 decreased in solution (Fig. 1d). Aside from PO_4, no other analyte showed a significant difference in its behavior upon introduction of U (Fig. 1). Sequential extraction showed that the same bicarbonate extraction step resulted in removal of both U and P (Fig. 6) at a ratio consistent with uranyl phosphate stoichiometry (P:U of 1.7 and 1.8, for 180d and 365d, respectively). Decrease in PO_4 in solution was correlated with initial U content, strongly suggesting that a precipitate with a PO_4/U ratio of 1 (accounting for PO_4 removal in the absence of added PO_4) controls the speciation of uranium in this system. This is confirmed by the detection of meta-ankoleite $K_2(UO_2)_2(PO_4)_2{\cdot}8H_2O$ (eq. (5), Gorman-Lewis et al., 2008) by XRD, TRILFS, SEM/EDX and EXAFS at all reaction times irrespective of initial U concentration (Table 1, Table 2, Fig. 2, Fig. 3, Fig. 4, Fig. 5).

$$(5)\quad 2K^+ + 2UO_2^{2+} + 2PO_4^{3-} + 8H_2O \rightarrow K_2(UO_2)_2(PO_4)\bullet 8H_2O$$

EXAFS spectra indicate that meta-ankoleite is not the only phase precipitating in this system, since linear combination fits indicate that meta-ankoleite speciation corresponds to about 50% of all U, and the remaining fraction is accounted for by boltwoodite, compreignacite, and becquerelite in various amounts.

As in the PO_4-reactant free system, thermodynamic modeling in the PO_4-amended system predicts that >90% of aqueous uranium is present as uranyl carbonate complexes and that the solution is oversaturated with respect to U phosphates, carbonates, silicates and metashoepite at 7 d (Fig. 7). After that time point, the solution is oversaturated with respect to only U phosphates until 365 d when it also becomes supersaturated with respect to uranyl silicates. Stability predictions based on solution composition suggest that hydrated uranium carbonate phases (grimselite, swartzite) are the dominant uranium phases in our experimental domain (Fig. S2b). However, similar to the PO_4-reactant free system, it appears that dissolved carbonate concentrations are increased by atmospheric equilibration, and some of this may have occurred post reaction. Upon subtracting the contributions of atmospheric CO_2 in-gassing, meta-ankoleite is predicted to be the most stable uranium phase in our experimental domain (Figs. S2d, S3b and d).

The persistence of oxyhydroxides (observed by EXAFS) after they appear to be thermodynamically unstable (Table 2) is noteworthy, and suggestive of kinetic limitations to their dissolution. Reinoso-Maset et al. (2017) observed

that in low (<0.5 mmol L^{-1}) carbonate systems, dissolution of uranyl hydroxides (compreignacite, becquerelite) was kinetically limited, which is consistent with their persistence in our system as well.

In model homogeneous nucleation experiments, where similar solutions as in our system were spiked with PO_4 or both PO_4 and Si, at various pH, Kanematsu et al. (2014) observed the precipitation of compreignacite followed by transformation to poorly-crystalline boltwoodite in the presence of Si at pH 5–7. In the presence of PO_4 and at all pH, they observed the precipitation of meta-ankoleite which transformed to phosphuranylite with time. These observations are very similar to those described here for complex sediments (and hence heterogeneous nucleation reactions). Similarly, during the weathering of sediments at acidic pH in the presence of U, Gartman et al. (2015) observed uranyl phosphates to be the dominant U species formed. The principal difference between these studies and the present one is the timing of Si incorporation into the uranium solid, limited, in the present case, by kinetics of dissolution of silicate minerals in the sediment.

5. Implications

The results of this study confirm the importance of dissolved phosphate as a control on U speciation in Hanford sediments, as suggested in model studies (Wellman et al., 2008, Kanematsu et al., 2014, Mehta et al., 2014). Here, the uranyl phosphate, meta-ankoleite, appears well crystallized and its low solubility will limit dissolved U(VI) concentrations in groundwater. Although the same is true for boltwoodite, its rate-limited precipitation in the absence of added PO_4 enables the initial precipitation of more soluble, less crystalline uranyl oxyhydroxides.

The presence of calcite in the Hanford vadose zone contributes to a rapid buffering of the solution pH from the starting pH of 3 to near neutral in a few days. Calcite-induced buffering of the ASCW solution superimposed with silicate weathering creates the geochemical conditions favorable for U stabilization in hydroxide phases and silicates in Hanford sediments. Although it is unclear whether PO_4 was consistently a constituent of the acidic crib waste streams at Hanford, our results suggest that when it was present at sufficient concentration, nearly all uranium would have precipitated in the upper soil in the form of meta-ankoleite (Fig. 6b). In the absence of added PO_4, however, fast infiltration rates would likely have prevented the precipitation of stable uranium silicate phase by mobilizing Si down the soil profile.

More generally, the results show a strong coupling between weathering of primary minerals and speciation/sequestration of uranium. Changes in speciation upon introduction of phosphate support previous observation that phosphate addition promotes U(VI) retention in soils (Pan et al., 2016). Such an amendment is therefore a good candidate for the sustainable remediation of U(VI) contamination in soils as suggested in Fuller et al., 2003, Wellman et

al., 2007 and Pan et al. (2016). Precipitation of uranyl silicates further contributes to the long-term immobilization of U(VI). Taken together, results suggest that acidification combined with PO_4 addition could trigger a long-term significant immobilization of U(VI) into highly stable uranyl silicates in soils contaminated by U(VI).

Acknowledgments

We thank Mary Kay Amistadi for ICP-MS analysis, Phil Anderson for support at the SEM, Dr. Rob Root for help at the beamline and Grant Reeder for assistance in GWB modeling. This research was funded by the Subsurface Biogeochemical Research (SBR-DE-SC0006781) Program, Office of Science, U.S. Department of Energy. Portions of this research were carried out at the Stanford Synchrotron Radiation Lightsource, a national user facility operated by Stanford University on behalf of the U.S. Department of Energy, Office of Basic Energy Sciences. We thank the SLAC radiation protection program for their assistance with radioactive sample handling.

References

Ainsworth et al., 2005

C.C. Ainsworth, J.M. Zachara, K. Wagnon, S. McKinley, C. Liu, S.C. Smith, H.T. Schaef, P.L. Gassman**Impact of highly basic solutions on sorption of Cs+ to subsurface sediments from the Hanford site, USA**

Geochim. Cosmochim. Acta, 69 (2005), pp. 4787-4800

Alwan and Williams, 1980

A.K. Alwan, P.A. Williams**The aqueous chemistry of uranium minerals. Part 2. Minerals of the liebigite group**

Mineral. Mag., 43 (1980), pp. 665-667

Arai et al., 2007

Y. Arai, M.K. Marcus, N. Tamura, J.A. Davis, J.M. Zachara**Spectroscopic evidence for uranium bearing precipitates in vadose zone sediments at the Hanford 300-area site**

Environ. Sci. Technol., 41 (2007), pp. 4633-4639

Begin and Fortin, 2003

L. Begin, J. Fortin**Evaluation of an acid ammonium oxalate extraction to determine fluoride resident concentrations in soils**

J. Environ. Qual., 32 (2003), pp. 662-673

Bickmore et al., 2001

B.R. Bickmore, K.L. Nagy, J.S. Young, J.W. Drexler**Nitrate-cancrinite precipitation on quartz sand in simulated Hanford tank solutions**

Environ. Sci. Technol., 35 (2001), pp. 4481-4486

Brantley, 2008

S.L. Brantley**Kinetics of mineral dissolution**

S.L. Brantley, J.D. Kubicki, A.F. White (Eds.), Kinetics of Water-rock Interaction, Springer (2008), pp. 151-210

Brown et al., 2010

C.F. Brown, R.J. Serne, J.G. Catalano, K.M. Krupka, J.P. Icenhower**Mineralization of contaminant uranium and leach rates in sediments from Hanford, Washington**

Appl. Geochem., 25 (2010), pp. 97-104

Burns, 2007

P. Burns**Crystal chemistry of uranium oxocompounds: an overview**

K. S.V., B. P.C., T. I.G. (Eds.), Structural Chemistry of Inorganic Compounds, Elsevier (2007), pp. 1-30

Casey et al., 1989

W.H. Casey, H.R. Westrich, G.W. Arnold, J.F. Banfield**The surface-chemistry of dissolving labradorite feldspar**

Geochim. Cosmochim. Acta, 53 (1989), pp. 821-832

Catalano et al., 2004

J.G. Catalano, S.M. Heald, J.M. Zachara, G.E. Brown**Spectroscopic and diffraction study of uranium speciation in contaminated vadose zone sediments from the Hanford site, Washington state**

Environ. Sci. Technol., 38 (2004), pp. 2822-2828

Catalano et al., 2006

J.G. Catalano, J.P. McKinley, J.M. Zachara, S.M. Heald, S.C. Smith, G.E. Brown **Changes in uranium speciation through a depth sequence of contaminated Hanford sediments**

Environ. Sci. Technol., 40 (2006), pp. 2517-2524

CH2MHILL, 2005

CH2MHILL**Hanford soil Inventory Model, Rev. 1**

Pacific Northwest National Laboratory. PNNL, Richland, Washington (2005)

Chang et al., 2011

H.-S. Chang, W. Um, K. Rod, R.J. Serne, A. Thompson, N. Perdrial, C.I. Steefel, J. Chorover**Strontium and cesium release mechanisms during unsaturated flow through waste-weathered Hanford sediments**

Environ. Sci. Technol., 45 (2011), pp. 8313-8320

Chen et al., 1999

F. Chen, R.C. Ewing, S.B. Clark**The Gibbs free energies and enthalpies of formation of U^{6+} phases: an empirical method of prediction**

Am. Mineralogist, 84 (1999), pp. 650-664

Chorover et al., 2008

J. Chorover, S. Choi, P. Rotenberg, R.J. Serne, N.A. Rivera, C. Strepka, A. Thompson, K.T. Mueller, P.A. O'Day**Silicon control of strontium and cesium partitioning in hydroxide-weathered sediments**

Geochim. Cosmochim. Ac, 72 (2008), pp. 2024-2047

DOE, 2010

U.S. DOE**216-U-8 Crib and 216-U-12Crib Vadose Zone Characterization Sampling and Analysis Plan**

Department of Energy (2010)

DOE, 2012

U.S. DOE**Hanford Site: Third CERCLA Five-year Review Report**

U.S. Department of Energy, Richland Operations Office (2012), p. 204

Dold, 2003

B. Dold**Speciation of the most soluble phases in a sequential extraction procedure adapted for geochemical studies of copper sulfide mine waste**

J. Geochem. Explor., 80 (2003), pp. 55-68

Downs and Hall-Wallace, 2003

R.T. Downs, M. Hall-Wallace**The American mineralogist crystal structure database**

Am. Mineralogist, 88 (2003), pp. 247-250

Duff et al., 2002

M.C. Duff, J.U. Coughlin, D.B. Hunter**Uranium co-precipitation with iron oxide minerals**

Geochim. Cosmochim. Acta, 66 (2002), pp. 3533-3547

Fenter et al., 2003

P. Fenter, C. Park, L. Cheng, Z. Zhang, M.P.S. Krekeler, N.C. Sturchio**Orthoclase dissolution kinetics probed by in situ X-ray reflectivity: effects of temperature, pH, and crystal orientation**

Geochim. Cosmochim. Acta, 67 (2003), pp. 197-211

Fuller et al., 2003

C.C. Fuller, J.R. Bargar, J.A. Davis**Molecular-scale characterization of uranium sorption by bone apatite materials for a permeable reactive barrier demonstration**

Environ. Sci. Technol., 37 (2003), pp. 4642-4649

Gartman et al., 2015

B.N. Gartman, N.P. Qafoku, J.E. Szecsody, R.K. Kukkadapu, Z. Wang, D.M. Wel lman, M.J.Truex**Uranium fate in Hanford sediment altered by simulated acid waste solutions**

Appl. Geochem., 63 (2015), pp. 1-9

George and Pickering, 2000

G.N. George, I.J. Pickering**EXAFSPAK: a Suite of Computer Programs for Analysis of X-ray Absorption Spectra**

Stanford Synchrotron Radiation Laboratory (2000)

Gorman-Lewis et al., 2008

D. Gorman-Lewis, J.B. Fein, P.C. Burns, J.E.S. Szymanowski, J. Convers e**Solubility measurements of the uranyl oxide hydrate phases metaschoepite, compreignacite, Na-compreignacite, becquerelite, and clarkeite**

J. Chem. Thermodyn., 40 (2008), pp. 980-990

Gražulis et al., 2009

S. Gražulis, D. Chateigner, R.T. Downs, A.T. Yokochi, M. Quirós, L. Lutterotti, E. Majnakova, J. Butkus, P. Moeck, A. Le Bail**Crystallography Open Database - an open-access collection of crystal structures**

J. Appl. Crystallogr., 42 (2009)

Gražulis et al., 2012

S. Gražulis, A. Daškevič, A. Merkys, D. Chateigner, L. Lutterotti, M. Quirós, N. R.Serebryanaya, P. Moeck, R.T. Downs, A. Le Bail**Crystallography Open Database (COD): an open-access collection of crystal structures and platform for world-wide collaboration**

Nucleic Acids Res., 40 (2012), pp. D420-D427

Grenthe et al., 1992

I. Grenthe, J. Fuger, R. Konings, R. Lemire, A. Muller, C. Nguyen-Trung, H. Wa nner**Chemical Thermodynamics of Uranium**

Elsevier & OECD Nuclear Energy Agency (1992)

Guillaumont et al., 2003

R. Guillaumont, T. Fanghanel, J. Fuger, I. Grenthe, V. Neck, D.A. Palmer, M.H. Rand**Update on the Chemical Thermodynamics of Uranium, Neptunium, Plutonium, Americium and Technetium**

Elsevier & OECD Nuclear Energy Agency (2003)

Hellmann, 1997

R. Hellmann**The albite-water system .4. Diffusion modeling of leached and hydrogen-enriched layers**

Geochim. Cosmochim. Acta, 61 (1997), pp. 1595-1611

Hellmann et al., 2012

R. Hellmann, R. Wirth, D. Daval, J.-P. Barnes, J.-M. Penisson, D. Tisserand, T. E picier, B.Florin, R.L. Hervig**Unifying natural and laboratory chemical weathering with interfacial dissolution–reprecipitation: a study based on the nanometer-scale chemistry of fluid–silicate interfaces**

Chem. Geol., 294–295 (2012), pp. 203-216

Hochella et al., 1988

M.F. Hochella, H.B. Ponader, A.M. Turner, D.W. Harris**The complexity of mineral dissolution as viewed by high resolution scanning Auger microscopy: labradorite under hydrothermal conditions**

Geochim. Cosmochim. Acta, 52 (1988), pp. 385-394

https

https://energy.gov/em/hanford-site, website operated by the U.S. Department of Energy, accessed 10/25/2017.

Kanematsu et al., 2014

M. Kanematsu, N. Perdrial, W. Um, J. Chorover, P.A. O'Day**Influence of phosphate and silica on U(VI) precipitation from acidic and neutralized wastewaters**

Environ. Sci. Technol., 48 (2014), pp. 6097-6106

Lande et al., 2007-2010

J. Lande, S. Webb, A. Mehta**Area Diffraction Machine Software**

(2007-2010)

Maher et al., 2013

K. Maher, J.R. Bargar, G.E. Brown Jr.**Environmental speciation of actinides**

Inorg. Chem., 52 (2013), pp. 3510-3532

Mantha et al., 2012

N.M. Mantha, M. Schindler, M. Murayama, M.F. Hochella**Silica- and sulfate-bearing rock coatings in smelter areas: products of chemical weathering and atmospheric pollution I. Formation and mineralogical composition**

Geochim. Cosmochim. Acta, 85 (2012), pp. 254-274

Mashal et al., 2004

K. Mashal, J.B. Harsh, M. Flury, A.R. Felmy, H.T. Zhao**Colloid formation in Hanford sediments reacted with simulated tank waste**

Environ. Sci. Technol., 38 (2004), pp. 5750-5756

McKeague and Day, 1966

J. McKeague, D. Day**Dithionite- and oxalate-extractable Fe and Al as aids in differentiating various classes of soils**

Can. J. Soil Sci., 46 (1966), pp. 13-22

McKinley et al., 2007

J.P. McKinley, J.M. Zachara, J. Wan, D.E. McCready, S.M. Heald**Geochemical controls on contaminant uranium in vadose Hanford formation sediments at the 200 area and 300 area, Hanford Site, Washington**

Vadose Zone J., 6 (2007), pp. 1004-1017

Mehta et al., 2014

V.S. Mehta, F. Maillot, Z.M. Wang, J.G. Catalano, D.E. Giammar**Effect of co-solutes on the products and solubility of uranium (VI) precipitated with phosphate**

Chem. Geol., 364 (2014), pp. 66-75

Murakami et al., 2005

T. Murakami, T. Sato, T. Ohnuki, H. Isobe**Field evidence for uranium nanocrystallization and its implications for uranium transport**

Chem. Geol., 221 (2005), pp. 117-126

Nesbitt and Muir, 1988

H.W. Nesbitt, I.J. Muir**SIMS depth profiles of weathered plagioclase and processes affecting dissolved Al and Si in some acidic soil solutions**

Nature, 334 (1988), pp. 336-338

Oelkers et al., 2009

E.H. Oelkers, S.V. Golubev, C. Chairat, O.S. Pokrovsky, J. Schott**The surface chemistry of multi-oxide silicates**

Geochim. Cosmochim. Acta, 73 (2009), pp. 4617-4634

Pan et al., 2016

Z. Pan, D.E. Giammar, V. Mehta, L.D. Troyer, J.G. Catalano, Z. Wang**Phosphate-induced immobilization of uranium in Hanford sediments**

Environ. Sci. Technol., 50 (2016), pp. 13486-13494

Perdrial et al., 2011

N. Perdrial, N. Rivera, A. Thompson, P. O'Day, J. Chorover**Trace contaminant concentration affects mineral transformation and pollutant fate in hydroxide-weathered Hanford sediments**

J. Hazard. Mater., 197 (2011), pp. 119-127

Perdrial et al., 2014

N. Perdrial, A. Thompson, P.A. O'Day, C.I. Steefel, J. Chorover**Mineral transformation controls speciation and pore-fluid transmission of contaminants in waste-weathered Hanford sediments**

Geochim. Cosmochim. Acta, 141 (2014), pp. 487-507

Plummer and Busenberg, 1987

L.N. Plummer, E. Busenberg**Thermodynamics of aragonite-strontianite solid-solutions - results from stoichiometric solubility at 25-degrees-C and 76-degrees-C**

Geochim. Cosmochim. Acta, 51 (1987), pp. 1393-1411

Qafoku et al., 2004

N.P. Qafoku, C.C. Ainsworth, J.E. Szecsody, O.S. Qafoku**Transport-controlled kinetics of dissolution and precipitation in the sediments under alkaline and saline conditions**

Geochim. Cosmochim. Acta, 68 (2004), pp. 2981-2995

Ravel and Newville, 2005

B. Ravel, M. Newville**Athena, Artemis, Hephaestus: data analysis for X-ray absorption spectroscopy using IFEFFIT**

J. Synchrotron Radiat., 12 (2005), pp. 537-541

Reinoso-Maset et al., 2017

E. Reinoso-Maset, C.I. Steefel, W. Um, J. Chorover, P. O'Day**Rates and mechanisms of uranyl oxyhydroxide mineral dissolution**

Geochim. Cosmochim. Acta, 207 (2017), pp. 198-321

Riley and Zachara, 1992

R.G. Riley, J.M. Zachara**Chemical Contaminants on DOE Lands and Selection of Contaminant Mixtures for Subsurfaces Sciences Research**

U.S. Department of Energy, Office of Energy Research, Washington, DC, USA (1992)

Rod et al., 2010

K.A. Rod, W. Um, M. Flury**Transport of strontium and cesium in simulated Hanford tank waste leachate through quartz sand under saturated and unsaturated flow**

Environ. Sci. Technol., 44 (2010), pp. 8089-8094

Rod et al., 2012

K.A. Rod, D.M. Wellman, M. Flury, E.M. Pierce, J.B. Harsh**Diffusive release of uranium from contaminated sediments into capillary fringe pore water**

J. Contam. Hydrol., 140 (2012), pp. 164-172

Schweda et al., 1997

P. Schweda, L. Sjoberg, U. Sodervall**Near-surface composition of acid-leached labradorite investigated by SIMS**

Geochim. Cosmochim. Acta, 61 (1997), pp. 1985-1994

Singer et al., 2009

D.M. Singer, J.M. Zachara, G.E. Brown**Uranium speciation as a function of depth in contaminated Hanford sediments - a micro-XRF, micro-XRD, and micro- and bulk-XAFS study**

Environ. Sci. Technol., 43 (2009), pp. 630-636

Stubbs et al., 2009

J.E. Stubbs, L.A. Veblen, D.C. Elbert, J.M. Zachara, J.A. Davis, D.R. Veblen**New ly recognized hosts for uranium in the Hanford Site vadose zone**

Geochim. Cosmochim. Acta, 73 (2009), pp. 1563-1576

Tang et al., 2013

G. Tang, W. Luo, D.B. Watson, S.C. Brooks, B. Gu**Prediction of aluminum, uranium, and co-contaminants precipitation and adsorption during titration of acidic sediments**

Environ. Sci. Technol., 47 (2013), pp. 5787-5793

Thompson et al., 2010

A. Thompson, C.I. Steefel, N. Perdrial, J. Chorover**Contaminant desorption during long-term leaching of hydroxide-weathered hanford sediments**

Environ. Sci. Technol., 44 (2010), pp. 1992-1997

Um et al., 2010

W. Um, J.P. Icenhower, C.F. Brown, R.J. Serne, Z.M. Wang, C.J. Dodge, A.J. Francis**Characterization of uranium-contaminated sediments from beneath a nuclear waste storage tank from Hanford, Washington: implications for contaminant transport and fate**

Geochim. Cosmochim. Acta, 74 (2010), pp. 1363-1380

Um et al., 2009

W. Um, Z.M. Wang, R.J. Serne, B.D. Williams, C.F. Brown, C.J. Dodge, A.J. Francis**Uranium phases in contaminated sediments below Hanford's U tank farm**

Environ. Sci. Technol., 43 (2009), pp. 4280-4286

Wan et al., 2004

J.M. Wan, T.K. Tokunaga, J.T. Larsen, R.J. Serne**Geochemical evolution of highly alkaline and saline tank waste plumes during seepage through vadose zone sediments**

Geochim. Cosmochim. Acta, 68 (2004), pp. 491-502

Webb, 2010

S.M. Webb**SixPACK: Sam's Interface for XAS Package**

(2010)

http://home.comcast.net/~sam_webb/sixpack.html

Wellman et al., 2007

D.M. Wellman, E.M. Pierce, M.M. Valenta**Efficacy of soluble sodium tripolyphosphate amendments for the in-situ immobilization of uranium**

Environ. Chem., 4 (2007), pp. 293-300

Wellman et al., 2008

D.M. Wellman, J.N. Glovack, K. Parker, E.L. Richards, E.M. Pierce**Sequestration and retention of U(VI) in presence of hydroxylapatite under dynamic geochemical conditions**

Environ. Chem., 5 (2008), pp. 40-50

Wronkiewicz et al., 1992

D.J. Wronkiewicz, J.K. Bates, T.J. Gerding, E. Veleckis, B.S. Tani**Uranium release and secondary phase formation during unsaturated testing of UO2 at 90-degrees-C**

J. Nucl. Mater, 190 (1992), pp. 107-127

Zachara et al., 2007

Zachara, J.M., Serne, R.J., Freshley, M.D., Mann, F.M., Anderson, F., Wood, M., Jones, T., Myers, D.A. (2007) Geochemical processes controlling migration of tank wastes in.

Zhou and Gu, 2005

P. Zhou, B.H. Gu**Extraction of oxidized and reduced forms of uranium from contaminated soils: effects of carbonate concentration and pH**

Environ. Sci. Technol., 39 (2005), pp. 4435-4440